Hysteretic optomagnetic bistability based on the plasmon-induced inverse Faraday effect in magnetoplasmonic disk resonators

Kum-Song Ho, Song-Jin Im ⬥,* Chol-Song Ri, Ji-Song Pae, and Gil-Song Song

Department of Physics, Kim Il Sung University, Taesong District, 02-381-4410 Pyongyang, Democratic People's Republic of Korea

We investigate the inverse Faraday effect (IFE) by surface plasmon traveling modes in an ultracompact magnetoplasmonic disk resonator side-coupled to a plasmonic waveguide. The magnetic field by the IFE reacts to the traveling modes and leads to a nonlinear shift of the resonance in the disk resonator. Describing those nonlinear phenomena analytically by using the temporal coupled mode theory and the Lorentz reciprocity theorem, we propose a conception of hysteretic optomagnetic bistability that the system has two stable states of optically induced magnetic field to switch on and off, depending upon the history of the incident optical power. The numerical simulations agree well with the analytical prediction. The proposed conception may find potential applications in all-optical magnetic recording and switching with nanometer resolution.

Optical bistability is a nonlinear optical phenomenon, and when it occurs, the optical system has two stable states for a certain intensity of the external field. Based on this phenomenon, many researchers have suggested various useful optical devices such as optical memories [1,2], optical transistors [3,4], and optical switches [5–8], and optical logic gates [9,10]. For a manifestation of optical bistability, one needs two factors, nonlinearity and feedback, which is often provided by a resonator. With the introduction of a plasmonic structure, which has good advantages due to its intrinsic tight confinement of field and plasmon resonance, one can highly enhance the optical nonlinearity on a subwavelength scale [11–14]. Furthermore, a nanoresonator coupled to a plasmonic waveguide is one of the ideal structures to achieve highly integrated optical chips by its nanofabrication flexibility and high-quality resonance [15].

The inverse Faraday effect (IFE) is an optomagnetic effect where circularly polarized light can act as an effective magnetic field along the wave vector, and studies on it have opened new possibilities for ultrafast magnetic recording and switching [16–18]. In recent years, plasmonic structures have been studied for the enhancement of the IFE [19–22] and for all-optical control of the magnetization with nanometer resolution [23–25]. Especially, an effective magnetic field can be induced by a free running surface plasmon polariton due to the IFE, instead of free space circularly polarized light [26–28]. The effective magnetic field can react to the surface plasmon polariton, leading to a different type of ultrafast third-order nonlinearity [26,28].

In this Rapid Communication, we study the bistability in a magnetoplasmonic system by IFE-related third-order nonlinearity. Recently, we investigated ultracompact magnetoplasmonic disk resonators with a high-quality factor by plasmon resonance enhancement combined with resonator resonance

enhancement [29,30]. A disk resonator side-coupled to a plasmonic waveguide supports a traveling wave mode which induces an effective magnetic field along the direction perpendicular to the disk surface due to the plasmon-induced IFE. It reacts to the traveling modes and leads to a nonlinear shift of the resonance. Due to this nonlinearity, the magnetoplasmonic disk resonator manifests the bistability in that the system has two magnetic states for one value of incident optical power.

Figure 1 shows a magnetoplasmonic disk resonator side-coupled to a metal-insulator-metal (MIM) waveguide. Here, d is the distance between the resonator and the waveguide, and γ_0 and γ_e are decay rates of the resonator due to internal loss and the escape rate to the waveguide, respectively. ε_m and ε_d are permittivities of the metal and dielectric layers of the waveguide, respectively. For the ferromagnetic dielectric composing the magnetoplasmonic disk resonator, the electric displacement depends on an external magnetic field according to the following relation,

$$\vec{D} = \varepsilon_0 \hat{\varepsilon} \vec{E} = \varepsilon_0 (\varepsilon_r \vec{E} + i\alpha \vec{E} \times \vec{M}), \quad (1)$$

where $\hat{\varepsilon}$ is the permittivity tensor, ε_r is its diagonal component, α is the magneto-optical susceptibility, and $\vec{M}$ is the magnetization.

For the magnetoplasmonic disk resonator, a transverse magnetic (TM) surface plasmon traveling mode can be excited by directional coupling between the disk resonator and the plasmonic waveguide. The rotating electric field vector of the TM mode can act as an effective magnetic field along the transverse $\hat{y}$ direction due to the plasmon-induced IFE [26–28], which is expressed as follows,

$$\vec{H}_{\mathrm{eff}} = -i\varepsilon_0 \alpha \vec{E} \times \vec{E}^* = -i\varepsilon_0 \alpha (E_x^* E_z - E_x E_z^*)\hat{y}. \quad (2)$$

The induced magnetic field reacts to the traveling modes and leads to a nonlinear shift of the wave number of the TM surface plasmon traveling mode. The nonlinear shift of the traveling mode wave number can be calculated by using the Lorentz reciprocity theorem [26] (see the detailed derivation

*sj.im@ryongnamsan.edu.kp
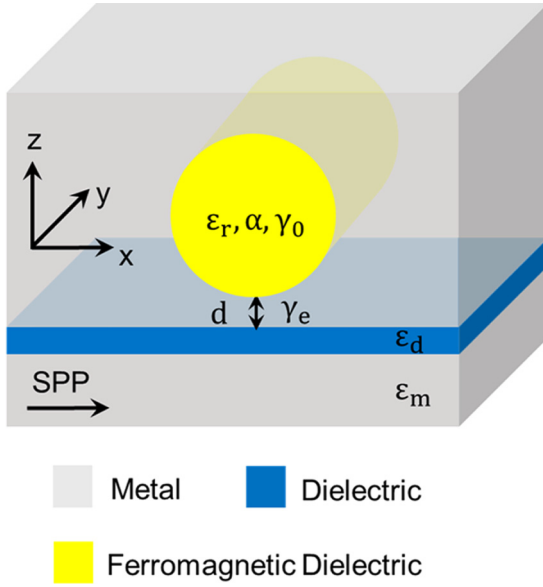
FIG. 1. The scheme of a magnetoplasmonic disk resonator coupled to a metal-insulator-metal waveguide. Here, ε_r is the linear permittivity of the ferromagnetic dielectric, and α is the magneto-optical susceptibility.

FIG. 2. Number of roots of Eq. (7) according to the normalized detuning Δ and the incident power P_{in}.

in the Supplemental Material [31]),

$$\Delta k = \frac{\int \alpha^2 E_x E_z (E_x^* E_z - E_x E_z^*) ds}{Z_0^3 \int (\vec{E} \times \vec{H}) \cdot \hat{x} ds} k_0, \quad (3)$$

where $Z_0 = \sqrt{\mu_0/\varepsilon_0} \approx 377 \ \Omega$ and $k_0 = \omega/c$ are the vacuum wave impedance and wave number, respectively. ε_0 and μ_0 are the vacuum permittivity and permeability, respectively.

Let us assume that an incident wave with frequency ω and power P_{in} is propagating through the waveguide. Then, the energy of the resonator $W(\omega, P_{in})$ can be expressed by the incident power P_{in} by using the temporal coupled mode theory [32] as follows (see the detailed derivation in the Supplemental Material [31]),

$$W(\omega, P_{in}) = \frac{2\gamma_0}{(\omega - \omega_0)^2 + 4\gamma_0^2} P_{in}. \quad (4)$$

Here, ω_0 is the resonance frequency of the resonator and we assumed that $\gamma_e/\gamma_0 = 1$, which can be realized by adjusting the distance d. γ_e is the escape rate due to the coupling between the waveguide and the resonator and mainly depends on the distance d between the waveguide and the disk resonator. In general, γ_e exponentially decreases with increasing d. On the other hand, γ_0 is the decay rate due to the absorption in the resonator and does not strongly depend on the distance d. Thus, the condition $\gamma_e/\gamma_0 = 1$ can be realized by adjusting the distance d. For our specific simulations this condition is satisfied at the distance $d = 20$ nm.

If we consider that the energy of the resonator W can be expressed as $W = W_E + W_H = 1/2 \, \mathrm{Re}[d\omega\varepsilon(\omega)/d\omega]_{\omega_0} \int \varepsilon_0 |\vec{E}|^2 dsdl + 1/2 \int \mu_0 |\vec{H}|^2 dsdl$ [33], Eq. (3) is rewritten as follows from Eq. (4) (see the detailed derivation in the Supplemental Material [31]),

$$\Delta k = \frac{k_0}{\mu_0} \frac{\alpha^2}{\sigma_1 l} \frac{2\gamma_0}{(\omega - \omega_0)^2 + 4\gamma_0^2} P_{in},$$

$$\sigma_1 = \frac{Z_0 \int (\vec{E} \times \vec{H}) \cdot \hat{x} ds \{ \mathrm{Re}[d\omega\varepsilon(\omega)/d\omega]_{\omega_0} \int |\vec{E}|^2 ds + Z_0^2 \int |\vec{H}|^2 ds \}}{2 \int E_x E_z (E_x^* E_z - E_x E_z^*) ds}, \quad (5)$$

where l is a perimeter of the resonator and σ_1 is an effective mode area related to the mode distribution of the resonator. The wave-number shift leads to a nonlinear resonance shift and the modulation of the resonance frequency ω_0 is expressed as follows [29] $[\omega_0 \to \omega_0(\omega, P_{in})]$,

$$\omega_0(\omega, P_{in}) = \omega_0 \left(1 + \frac{c\Delta k}{n_{eff}\omega_0} \right). \quad (6)$$

Here, n_{eff} is the effective refractive index of the traveling mode. If we define that $\delta = [\omega_0(\omega, P_{in}) - \omega_0]/2\gamma_0$ and $\Delta =$

$[\omega - \omega_0]/2\gamma_0$, Eq. (6) can be rewritten as follows,

$$\delta[(\Delta - \delta)^2 + 1] = \frac{Q^2 \alpha^2}{\mu_0 \omega_0 n_{eff} \sigma_1 l} P_{in}. \quad (7)$$

Here, $Q = \omega_0/2\gamma_0$ is the quality factor of the resonator.

Figure 2 shows the number of roots of Eq. (7) according to the normalized detuning Δ and the incident power P_{in}. At a power larger than P_c and a certain normalized detuning Δ larger than $\sqrt{3}$, the nonlinear disk resonator can have two or
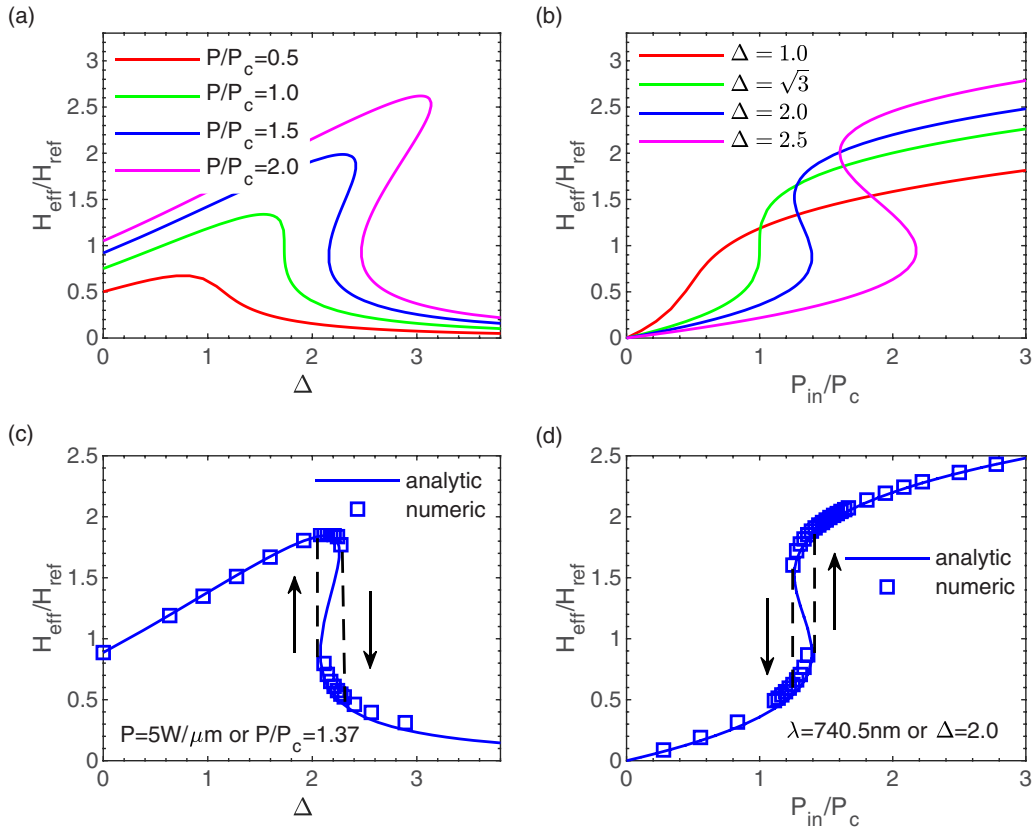
FIG. 3. The effective magnetic field induced in the resonator according to the normalized detuning Δ and the normalized waveguide powers P_{in}/P_c. (a) and (b) Analytical results from the roots of Eqs. (7) and (10). (c) and (d) Numerical simulation results compared with the above analytical results. (a) and (c) show the relation with the normalized detuning Δ for different P_{in}/P_c. (b) and (d) show the relation with P_{in}/P_c for different normalized detuning Δ.

three states. Here,

$$P_c = \frac{8\sqrt{3}\mu_0\omega_0}{9}\frac{n_{\text{eff}}\sigma_1 l}{Q^2\alpha^2}. \tag{8}$$

As you can see in Eq. (8), the critical power P_c, which determines the lowest power to realize multiple states, is inversely proportional to the squares of the magneto-optical susceptibility α and the quality factor Q and is proportional to the perimeter of the resonator l. The yellow curves in Fig. 2, which are boundaries between the conditions for the single state and the multiple states, are determined by

$$P_{\text{in}} = P_c[\Delta^3 + 9\Delta \pm (\Delta^2 - 3)^{3/2}]/12\sqrt{3}. \tag{9}$$

These optical multiple states of the resonator can lead to multiple states of optically induced magnetization in the resonator. From Eqs. (2) and (4), the induced effective magnetic field H_{eff} by the IFE can be described as follows,

$$\frac{H_{\text{eff}}}{H_{\text{ref}}} = \frac{4}{3[(\Delta - \delta)^2 + 1]}\frac{P_{\text{in}}}{P_c},$$

$$H_{\text{ref}} = \frac{4\mu_0}{\sqrt{3}}\frac{n_{\text{eff}}\sigma_1}{\sigma_2}\frac{1}{Q\alpha},$$

$$\sigma_2 = \frac{\text{Re}[d\omega\varepsilon(\omega)/d\omega]_{\omega_0}\int |\vec{E}|^2 ds + Z_0^2\int |\vec{H}|^2 ds}{\text{Im}(E_x^* E_z - E_x E_z^*)}. \tag{10}$$

Here, H_{ref} is the effective magnetic field in the case of $P_{\text{in}} = P_c$ and $\Delta = \sqrt{3}$, and σ_2 is another kind of effective mode area related to the mode distribution of the resonator. We note that H_{eff} is a value of the effective magnetic field near the interface and the effective magnetic field exponentially decreases along the direction perpendicular to the interface of the resonator, which can be seen in Fig. 4. If we substitute the analytical mode distributions in the planar metal-dielectric interface [33] to Eqs. (8) and (10), P_c and H_{ref} are expressed as follows,

$$P_c = \frac{-4\sqrt{3}Z_0(\varepsilon_r - \varepsilon_m)^{1/2}\varepsilon_m}{9}\left(\frac{1}{Q\alpha}\right)^2 l,$$

$$H_{\text{ref}} = \frac{4\mu_0(-\varepsilon_m\varepsilon_r)^{1/2}}{\sqrt{3}}\frac{1}{Q\alpha}. \tag{11}$$

Figure 3 shows the optomagnetic bistability predicted by Eqs. (7) and (10). We note that the system has only two stable states among three possible states, which means that once it is close to one of its stable states the system will rapidly switch to the stable one. The bistability begins to appear at $P_{\text{in}}/P_c = 1$ [see Fig. 3(a)] and at $\Delta = \sqrt{3}$ [see Fig. 3(b)]. The analytical results [the blue curves of Figs. 3(c) and 3(d)] agree well with the numerical simulation results [the blue squares of Figs. 3(c) and 3(d)]. In the numerical simulation, the experimental data of the permittivity of silver [34] have been used as the metal permittivity ε_m, the experimental data of the permittivity and the magneto-optical susceptibility of
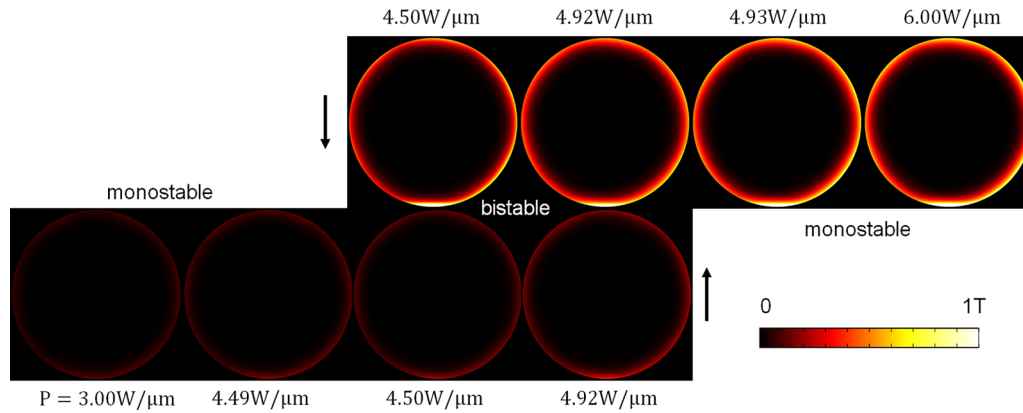
FIG. 4. Numerical simulation results of distributions of the effective magnetic field H_{eff} in the resonator for the case of Fig. 3(d).

Bi-substituted iron garnet (BIG) [22,35,36] have been used as ε_r and α, respectively ($\varepsilon_r = 8$, $\alpha = 5.5 \times 10^{-7}$ m/A), and the radius of the resonator $r = 400$ nm and the distance $d = 20$ nm between the waveguide and the resonator have been assumed. For these parameters the resonance wavelength of the resonator at a very low power is $\lambda_0 = 747$ nm and the condition $\Delta > \sqrt{3}$ is satisfied at a wavelength smaller than 741.6 nm. The reference effective magnetic field $H_{\text{ref}} \approx 0.3$ T and the critical power $P_c \approx 3.6$ W/μm, which are calculated from Eq. (11), have been assumed in Figs. 3(c) and 3(d). At a wavelength of 740.5 nm, two stable states are present in a power range from $P_{\min} = 4.50$ W/μm to $P_{\max} = 4.92$ W/μm corresponding to the normalized powers of 1.23 and 1.38 as shown in Fig. 3(d), which agree well with the analytical predictions from Eq. (9). The nonlinear resonator manifests a hysteretic behavior as shown in Figs. 3(c) and 3(d), which is promising for all-optical magnetic recording.

Figure 4 shows numerical simulation results of distributions of the effective magnetic field H_{eff} in the resonator for the case of Fig. 3(d). When the incident power P_{in} has a value from 4.50 to 4.92 W/μm, the resonator manifests

the bistability and it has one of two stable strong or weak magnetization states, depending on the initial state of the resonator. Also, one can see the high-contrast switching between the weak magnetization and the strong magnetization by smoothly controlling the incident power.

In conclusion, we proposed hysteretic optomagnetic bistability based on the plasmon-induced IFE in a magnetoplasmonic nanodisk resonator side-coupled to a plasmonic waveguide. We derived full-analytical expressions to describe the bistability of the resonator by using the temporal coupled mode theory and the Lorentz reciprocity theorem. The theoretical analysis predicts ways to reduce the critical power P_c for realizing the bistability, for example, it can be decreased by increasing the magneto-optical susceptibility α or the quality factor Q or by decreasing the resonance frequency ω_0 or the resonator perimeter l. The bistability is also critically affected by the detuning of the incident wavelength from the exact resonance. Numerical simulation results demonstrated the above theoretical predictions. Our results are promising for applications in all-optical magnetic recording and switching with nanometer resolution.

[1] L. Liu, R. Kumar, K. Huybrechts, T. Spuesens, G. Roelkens, E.-J. Geluk, T. de Vries, P. Regreny, D. V. Thourhout, R. Baets, and G. Morthier, Nat. Photonics **4**, 182 (2010).

[2] I. D. Rukhlenko, M. Premaratne, and G. P. Agrawal, Opt. Lett. **35**, 55 (2010).

[3] M. F. Yanik, S. Fan, M. Soljačić, and J. D. Joannopoulos, Opt. Lett. **28**, 2506 (2003).

[4] V. R. Tuz and S. L. Prosvirnin, J. Opt. Soc. Am. B **28**, 1002 (2011).

[5] M. Soljačić, M. Ibanescu, S. G. Johnson, Y. Fink, and J. D. Joannopoulos, Phys. Rev. E **66**, 055601(R) (2002).

[6] M. F. Yanik, S. Fan, and M. Soljačić, Appl. Phys. Lett. **83**, 2739 (2003).

[7] H. Lu, X. Liu, L. Wang, Y. Gong, and D. Mao, Opt. Express **19**, 2910 (2011).

[8] X.-S. Lin, J.-H. Yan, Y.-B. Zheng, L.-J. Wu, and S. Lan, Opt. Express **19**, 9594 (2011).

[9] F. D. le Coarer, M. Sciamanna, A. Katumba, M. Freiberger, J. Dambre, P. Bienstman, and D. Rontani, IEEE J. Sel. Top. Quantum Electron. **24**, 1 (2018).

[10] M. Amin, M. Farhat, and H. Bağcı, Opt. Express **22**, 6966 (2014).

[11] C. Argyropoulos, C. Ciracì, and D. R. Smith, Appl. Phys. Lett. **104**, 063108 (2014).

[12] P.-Y. Chen, C. Argyropoulos, and A. Alù, Nanophotonics **1**, 221 (2012).

[13] M. Kauranen and A. V. Zayats, Nat. Photonics **6**, 737 (2012).

[14] C. Argyropoulos, P.-Y. Chen, G. D'Aguanno, N. Engheta, and A. Alù, Phys. Rev. B **85**, 045129 (2012).

[15] G. Wang, H. Lu, X. Liu, Y. Gong, and L. Wang, Appl. Opt. **50**, 5287 (2011).

[16] E. Beaurepaire, J.-C. Merle, A. Daunois, and J.-Y. Bigot, Phys. Rev. Lett. **76**, 4250 (1996).

[17] C. D. Stanciu, F. Hansteen, A. V. Kimel, A. Kirilyuk, A. Tsukamoto, A. Itoh, and T. Rasing, Phys. Rev. Lett. **99**, 047601 (2007).

[18] A. Kirilyuk, A. V. Kimel, and T. Rasing, Rev. Mod. Phys. **82**, 2731 (2010).

[19] V. I. Belotelov, E. A. Bezus, L. L. Doskolovich, A. N. Kalish, and A. K. Zvezdin, J. Phys.: Conf. Ser. **200**, 092003 (2010).

[20] S. M. Hamidi, M. Razavinia, and M. M. Tehranchi, Opt. Commun. **338**, 240 (2015).

[21] C. von Korff Schmising, M. Giovannella, D. Weder, S. Schaffert, J. Webb, and S. Eisebitt, New J. Phys. **17**, 033047 (2015).

[22] A. Dutta, A. V. Kildishev, V. M. Shalaev, A. Boltasseva, and E. E. Marinero, Opt. Mater. Express **7**, 4316 (2017).

[23] D. Ignatyeva, C. Davies, D. Sylgacheva, A. Tsukamoto, H. Yoshikawa, P. Kapralov, A. Kirilyuk, V. Belotelov, and A. Kimel, Nat. Commun. **10**, 4786 (2019).

[24] T. Liu, T. Wang, A. H. Reid, M. Savoini, X. Wu, B. Koene, P. Granitzka, C. E. Graves, D. J. Higley, Z. Chen, G. Razinskas, M. Hantschmann, A. Scherz, J. Stohr, A.Tsukamoto, B. Hecht, A. V. Kimel, A. Kirilyuk, T. Rasing, and H. A. Durr, Nano Lett. **15**, 6862 (2015).

[25] A. L. Chekhov, A. I. Stognij, T. Satoh, T. V. Murzina, I. Razdolski, and A. Stupakiewicz, Nano Lett. **18**, 2970 (2018).

[26] S.-J. Im, C.-S. Ri, K.-S. Ho, and J. Herrmann, Phys. Rev. B **96**, 165437 (2017).

[27] S.-J. Im, J.-S. Pae, C.-S. Ri, K.-S. Ho, and J. Herrmann, Phys. Rev. B **99**, 041401(R) (2019).

[28] C.-S. Ri, S.-J. Im, J.-S. Pae, K.-S. Ho, Y.-H. Han, and J. Herrmann, Phys. Rev. B **100**, 155404 (2019).

[29] J.-S. Pae, S.-J. Im, K.-S. Ho, C.-S. Ri, S.-B. Ro, and J. Herrmann, Phys. Rev. B **98**, 041406(R) (2018).

[30] J.-S. Pae, S.-J. Im, C.-S. Ri, K.-S. Ho, G.-S. Song, Y.-H. Han, and J. Herrmann, Phys. Rev. B **100**, 041405(R) (2019).

[31] See Supplemental Material at http://link.aps.org/supplemental/10.1103/PhysRevB.101.041406 for detailed derivations and some additional information.

[32] C. Manolatou, M. J. Khan, S. Fan, P. R. Villenueve, H. A. Haus, and J. D. Joannopoulos, IEEE J. Quantum Electron. **35**, 1322 (1999).

[33] S. A. Maier, *Plasmonics: Fundamentals and Applications* (Springer, New York, 2007).

[34] P. B. Johnson and R. W. Christy, Phys. Rev. B **6**, 4370 (1972).

[35] S. Yao, R. Kamakura, S. Murai, K. Fujita, and K. Tanaka, J. Magn. Magn. Mater. **422**, 100 (2017).

[36] E. Popova, A. F. F. Galeano, M. Deb, B. Warot-Fonrose, H. Kachkachi, F. Gendron, F. Ott, B. Berini, and N. Keller, J. Magn. Magn. Mater. **335**, 139 (2013).